

Article

Real-Time Phase Bias Estimation for BeiDou Satellites Based on Consideration of Orbit Errors

Yanyan Liu ¹, Jiasong Zhu ^{1,*}, Shirong Ye ² and Weiwei Song ²

¹ Institute of Urban Smart Transportation & Safety Maintenance, College of Civil Engineering, Shenzhen University, Shenzhen 518060, China; whdxlyy@szu.edu.cn

² GNSS Research Center, Wuhan University, Wuhan 430079, China; shirongye_wuhu@163.com (S.Y.); weiweisong_wuhu@163.com (W.S.)

* Correspondence: jiasongzhu_szu@163.com

Received: 2 May 2018; Accepted: 7 June 2018; Published: 25 June 2018



Abstract: Correction of the fractional cycle bias (FCB) in the undifferenced ambiguity allows precise point positioning (PPP) integer ambiguity resolution (IAR) to be achieved, which can improve positioning accuracy significantly. In addition, in real-time PPP-IAR, integration of the BeiDou Navigation Satellite System (BDS) can provide a significant reduction in the initial fixing time of global positioning system (GPS)-only PPP-IAR. However, the FCB quality can be considerably affected by the low precision of the BDS orbit, which then severely hampers the GPS + BDS PPP-IAR performance. Therefore, a real-time FCB estimation strategy that takes the BDS satellite orbit error into consideration was developed in this study. The slant orbit error can be absorbed by the ionosphere-free (IF) ambiguity, which can then be recovered by fixing all IF ambiguities from all the tracking stations. The estimated orbit error is then used to refine the orbit, which is broadcast along with the FCBs to enable PPP ambiguity resolution. To evaluate the proposed strategy, an experiment using 60 tracking stations covering the China region is performed in a simulated real-time mode. The a posteriori residuals of both the wide- and narrow-lane ambiguities are checked to validate the efficiency of the proposed FCB strategy. The results show that when the proposed strategy is applied, the effect of the BDS orbit error on narrow-lane FCB estimation is eliminated and more than 94% of the narrow-lane residuals are within 0.1 cycles for both the GPS and the BDS. The fixing percentage within 20 min is 46.3% for the GPS-only solution but is only 4.8% when using GPS + BDS with the traditional method. However, when the proposed strategy is used, the fixing percentage for GPS + BDS improves significantly to 91.7%.

Keywords: GPS; BeiDou Navigation Satellite System (BDS); precise point positioning; ambiguity resolution; fractional cycle bias; orbit error

1. Introduction

By precise point positioning (PPP) [1], centimeter-level positioning accuracy with only a single receiver is achievable. PPP has been recognized as a powerful and efficient tool for many applications, including geophysics and meteorology [2–4]. While PPP has numerous advantages, it still takes approximately 30 min to achieve positioning solutions within accuracy of 10 cm. In addition, when compared with relative positioning, PPP suffers from relatively poor precision for observations covering a short time period.

In relative positioning, precise positioning can be achieved instantaneously using ambiguity resolution. In PPP, however, the uncalibrated phase delays (UPDs) [5], or alternatively, the fractional-cycle biases (FCBs) [6] are absorbed into the undifferenced ambiguity estimates; their integer properties are thus destroyed and therefore cannot be fixed. Fortunately, recent studies have demonstrated that suitable

integer resolutions can be achieved through application of improved satellite products in which the FCBs have been separated from the integer ambiguities [5,7–9]. While major achievements have been reported with regard to ambiguity-fixed PPP, the PPP technique still requires long convergence times of 30 min or more to obtain centimeter-level positioning accuracy or to produce its first ambiguity-fixed solution [10]. Such long convergence times are not acceptable for a wide range of applications.

Recently, some researchers proposed use of the Global Navigation Satellite System (GLONASS) to help with global positioning system (GPS) PPP ambiguity resolution. Jokinen et al. [11] studied the initial fixing time (IFT) improvements by adding GLONASS observations to help with GPS PPP ambiguity resolution, in which only the GPS ambiguity is fixed and GLONASS is left floating. Their results showed that the addition of GLONASS can reduce the IFT by approximately 5% when compared with GPS-only solutions. Li and Zhang [12] performed a similar analysis and found that the average IFT could be shortened by 27.4% in static mode and by 42.0% in kinematic mode. Later, other researchers analyzed the effects of simultaneous fixing of the GPS and GLONASS ambiguities; the results of Geng and Shi [13] showed that the fixing percentage within a 10-min period for kinematic PPP improved from 39.81 to 87.50%, while a similar improvement from 46.8 to 95.8% was reported by Liu et al. [14].

The BeiDou Navigation Satellite System (BDS) has been independently constructed and operated by China and has provided an official service in the Asia-Pacific region since 27 December 2012. The BDS satellite constellation is currently composed of five geostationary Earth orbit (GEO) satellites, five inclined geosynchronous satellite orbit (IGSO) satellites and four medium Earth orbit (MEO) satellites. Given the availability of precise clock and orbit products for the BDS satellites, it is therefore necessary to investigate the GPS + BDS PPP ambiguity resolution performance. It was shown in [15–17] that the convergence time of float PPP can be reduced by combining the observations from the BeiDou satellites. Liu et al. [18] showed that the fixing percentage for GPS-only kinematic precise point positioning integer ambiguity resolution (PPP-IAR) was 17.6% within a 10-min period, and this percentage improved to 42.8% following the addition of the IGSO and MEO satellites of the BDS. However, the fixing percentage degraded severely to 23.2% if the GEO satellites were included because of their low orbit accuracy. Researchers have performed large numbers of studies on precise orbit determination and precise positioning of the BDS [19–24]. However, because of the lack of sufficient numbers of tracking stations and a suitably precise solar radiation pressure model, the precision of the BDS orbit is low when compared with that of the GPS satellites, particularly for the GEO satellites, which have orbit errors of the order of 2–4 m. The Centre National d’Études Spatiales (CNES) has been providing real-time orbit and clock corrections for all global navigation satellite systems (GNSSs) since 2016. Kazmierski et al. [25] analyzed the quality of the CNES’s real-time orbit by comparing it with that of the final product from the Center for Orbit Determination in Europe (CODE) [26]. The results showed that GPS has the highest orbit precision of 2.3, 3.2, and 2.8 cm for its radial, along-track and cross-track components, respectively. For the BDS, the precision results for the three corresponding components were 12.1, 21.2, and 26.2 cm for the IGSO satellites and 4.8, 13.1, and 10.8 cm for the MEO satellites, respectively. To improve the precision of ultra-rapid orbits, Li et al. [27] used two days’ worth of data to perform multi-GNSS ultra-rapid orbit determination, and updated the orbit results every hour. The results showed that when compared with the traditional strategy, the overlap accuracies of the BDS GEO, IGSO, and MEO satellites can be improved by more than 50, 18, and 44% in the radial, cross-track, and along-track directions, respectively, and the root mean square (RMS) values are summarized in detail in Table 1.

Table 1. Overlap root mean square (RMS; units: m) values for ultra-rapid orbit. GEO: geostationary Earth orbit; IGSO: inclined geosynchronous satellite orbit; MEO: medium Earth orbit; GPS: global positioning system.

	GEO	IGSO	MEO	GPS
Along	0.690	0.160	0.150	0.032
Cross	0.170	0.085	0.042	0.019
Radial	0.101	0.065	0.035	0.010

As shown in Table 1, the accuracy of the BDS ultra-rapid orbit is very low and thus cannot satisfy the FCB estimation requirements. In this paper, we propose a new strategy for BDS FCB estimation in real time. We begin by addressing the fundamentals of simulated real-time PPP data processing. We then demonstrate how the satellite orbit will affect narrow-lane FCB estimation and provide a new narrow-lane FCB estimation strategy that takes satellite orbit errors into consideration. We use a network of 60 tracking stations to validate the proposed method. Finally, discussion and concluding remarks are presented based on our findings.

2. Methods

The well-known ionosphere-free (IF) combination is commonly used in satellite clock estimation and PPP processing to eliminate the first-order ionosphere delay. The IF carrier-phase and pseudorange observations between the satellite k and the receiver i can be written as:

$$\begin{aligned} P_{IF,i}^k &= \alpha P_{1,i}^k - \beta P_{2,i}^k = \rho_i^k + cdt_i - cdt^k + orb_i^k + e_{IF,i}^k \\ L_{IF,i}^k &= \alpha L_{1,i}^k - \beta L_{2,i}^k = \rho_i^k + cdt_i - cdt^k + N_{IF,i}^k + orb_i^k + \varepsilon_{IF,i}^k \end{aligned} \quad (1)$$

where $\alpha = f_1^{k2}/(f_1^{k2} - f_2^{k2})$ and $\beta = f_2^{k2}/(f_1^{k2} - f_2^{k2})$. P_i^k and L_i^k are the code and carrier phase observations, respectively, at frequency f^k . ρ_i^k is a nondispersive delay that includes the geometric delay, the tropospheric delay, and any other delay that has an identical effect on all observations. dt_i and dt^k are the receiver and satellite clock biases, respectively. c is the speed of light in a vacuum. $N_{IF,i}^k$ denotes the ambiguity of the IF carrier-phase observation. orb_i^k is the satellite orbit error mapped into the receiver-satellite direction, which is typically assessed using signal-in-space ranging error (SISRE) values [28]. The satellite-induced code bias (SICB) of the BDS must be corrected using e.g., the model reported by Wanninger and Beer (2015) [29]. Note that the GEO satellites can be corrected using the same model that is used for the IGSO satellites [30]. Finally, $e_{IF,i}^k$ and $\varepsilon_{IF,i}^k$ denote the unmodeled code and carrier phase errors, respectively, which include multipath effects and noise. Both the phase center correction and the phase windup effect [1,2,31] must be considered during the modeling process.

All real-time processes in this study are based on Equation (1). First, we fix the ultra-rapid orbit to enable estimation of the satellite clocks using a forward Kalman filter. To simulate a real-time scenario, we used the latest predicted orbits with 3 h of release latency. These clocks and the predicted orbits were then fixed as shown in the subsequent FCB estimation. Geng et al. [32] and Shi and Gao [33] have previously proved that the current PPP ambiguity resolution methods are equivalent in theoretical terms. Therefore, in this study, we focus solely on the method that was proposed by Ge et al. [5], in which the FCB determination is critical. Finally, the satellite's orbit, clock and FCB products are broadcast to all PPP users with a simulated latency of 3 s to assess the PPP-IAR performance.

2.1. Effects of Orbit Error on FCB Estimation

To generate the satellite FCB in PPP analysis, the satellite orbit and clock are fixed, which means that the orbit error is not separable from the IF ambiguity, and the second equation from Equation (1) will become:

$$L_{IF,i}^k = \rho_i^k + cdt_i - cdt^k + \tilde{N}_{IF,i}^k + \varepsilon_{IF,i}^k \quad (2)$$

where $\tilde{N}_{IF,i}^k = N_{IF,i}^k + orb_i^k$. The corresponding IF ambiguity can be expressed using a combination of the wide-lane (WL) and narrow-lane (NL) ambiguities for fixing:

$$\tilde{N}_{IF,i}^k = \frac{f_2^k}{f_1^k + f_2^k} \lambda_w^k N_{w,i}^k + \lambda_n^k (N_{n,i}^k + \phi_{n,i} - \phi_n^k + orb_i^k / \lambda_n^k) \quad (3)$$

where $N_{w,i}^k$ and $N_{n,i}^k$ are the WL and NL ambiguities, respectively, which have corresponding wavelengths of λ_w^k and λ_n^k . $\phi_{n,i}$ and ϕ_n^k are the receiver and satellite NL UPDs, respectively, and orb_i^k / λ_n^k is the NL orbit error.

In PPP, the WL ambiguity is usually resolved using the Hatch–Melbourne–Wübbena (HMW) combination [34–36] of the carrier phase and code observations as follows:

$$\begin{aligned}\tilde{N}_{w,i}^k &= \left(\frac{L_{1,i}}{\lambda_1} - \frac{L_{2,i}}{\lambda_2} - \frac{f_1^k P_{1,i}^k + f_2^k P_{2,i}^k}{(f_1^k + f_2^k) \lambda_w^k} \right) \\ &= N_{w,i}^k + \phi_{w,i} - \phi_w^k\end{aligned}\quad (4)$$

where $N_{w,i}^k$ is the integer WL ambiguity, and $\phi_{w,i}$ and ϕ_w^k are the receiver and satellite WL UPDs, respectively. The advantage of this approach is that it is not affected by atmospheric (ionosphere and troposphere) bias or any geometry-related bias. Therefore, it will not be affected by the orbit errors.

In high-precision satellite clock estimation, part of the orbital error can be compensated by the satellite clock, while the residual part will appear as code residuals or can be absorbed into the float IF ambiguity in PPP, which then goes into the NL ambiguity, as shown in Equation (3). According to Liu et al. [37], the proportion corresponding to the residual orbital error is governed by the term $2 \cdot |\sin(\theta/2)|$, which is called the scale factor. Here, θ represents the maximum value of the included angle between a vector from the satellite to one receiver and another vector from the same satellite to another receiver. The tracking network used in China covers an area with a radius of approximately 1500 km, and we can thus calculate the scale factor; then, based on the 3D orbit error given in Table 1, we can also calculate the effects of the residual orbital error on the NL ambiguity. The resulting values are summarized in Table 2. The results show that the orbit errors of the GPS satellites can be neglected, whereas the orbit errors of all three types of BDS satellites must be estimated along with the NL FCB parameters.

Table 2. Effects of orbit error on narrow-lane (NL) fractional cycle bias (FCB) estimation (RMS).

	3D Error (m)	Scale Factor	NL FCB (m)	NL FCB (Cycle)
GEO	0.718	0.0835	0.0599	0.599
IGSO	0.193	0.0835	0.0161	0.161
MEO	0.160	0.1390	0.0222	0.222
GPS	0.039	0.1477	0.0057	0.057

After the WL ambiguities are fixed, the float NL ambiguities can then be obtained using Equation (3):

$$\begin{aligned}\tilde{N}_{n,i}^k &= \left(\tilde{N}_{IF,i}^k - \frac{f_2^k}{f_1^k + f_2^k} \lambda_w^k N_{w,i}^k \right) / \lambda_n^k \\ &= N_{n,i}^k + \phi_{n,i} - \phi_n^k + orb_i^k / \lambda_n^k\end{aligned}\quad (5)$$

The orbit error is expressed as:

$$orb_i^k = l_i^k \cdot \Delta x^k + m_i^k \cdot \Delta y^k + n_i^k \cdot \Delta z^k \quad (6)$$

where Δx^k , Δy^k , and Δz^k are the satellite errors expressed in an Earth-centered and Earth-fixed coordinate system; and l_i^k , m_i^k and n_i^k are the corresponding direct cosines of the satellite.

To generate the GPS + BDS FCBs in the PPP analysis, the estimated parameters required include two receiver clock parameters, one zenith tropospheric delay (ZTD) parameter, and the undifferenced IF ambiguities. Based on the results given in Table 1, we can neglect the GPS orbit error; we therefore assign much less weight to the BDS observations so that the precision of both the ZTD parameter and the GPS receiver clock will not be affected by BDS orbital errors. The slant orbital error will therefore be absorbed by the BDS receiver clock and the IF ambiguities; the former can be compensated by

Table 3. GPS + BDS measurement model and parameter estimation strategy. BDS: BeiDou Navigation Satellite System; PPP: precise point positioning; IAR: precise point positioning integer ambiguity resolution; WL: wide lane.

Observation or Parameter	Model	Constraint
Observations	Undifferenced ionosphere-free code and carrier-phase combination; 30-s interval; 7° elevation cutoff	1 cm for carrier-phase and 1 m for pseudorange
Weight	Assign 100 times more weight for GPS in FCB estimation; equal weight for each system in PPP-IAR; elevation-dependent weighting	$E > 30^\circ$, 1; else $\sin(E)$
Phase center offset and variation of Satellite antenna	igs08_1899.atx for GPS and BDS	
Phase center offset and variation of Receiver antenna	igs08_1899.atx for GPS and use GPS values for BDS	
Phase rotation correction	Applied	
Site displacement	Solid Earth, pole tide, ocean loading [38]	
Troposphere	Saastamoinen model for wet and dry hydrostatic delay with global mapping function [39]	Initial model, 10 cm; random-walk process noise 2 cm/ \sqrt{hour}
Satellite orbit	International GNSS Monitoring & Assessment System (iGMAS) ultra rapid products for GPS and BDS (www.igmas.org)	
Receiver clock offset	Estimated for each system	White noise process
Relativistic effects	Applied	
WL and NL FCB	1-day update interval for WL and 5 min for NL; 1200-s initialization time for NL FCB	
Orbit error	15-min update interval with a 1200-s initialization time	
Receiver Coordinate	Fixed in satellite clock and FCB estimation while estimated in PPP	
Integer Ambiguity	Estimated as constant	Fixed for all GPS and BDS satellites

3. Data and Processing Strategy

The Positioning and Navigation Data Analyst (PANDA) software [40] that was developed at Wuhan University was used in this study and the proposed strategy is thus implemented in PANDA. Observations collected with 60 stations on days of the year (DOYs) 74–80, 2015 were processed, where 40 stations were used as reference stations for the satellite clock and FCB estimation, and the remaining 20 stations were used as rover stations to perform the PPP ambiguity resolution. Figure 1 shows the distribution of the stations used. The detailed processing strategies used for GPS + BDS FCB estimation and PPP ambiguity resolution are summarized in Table 1.

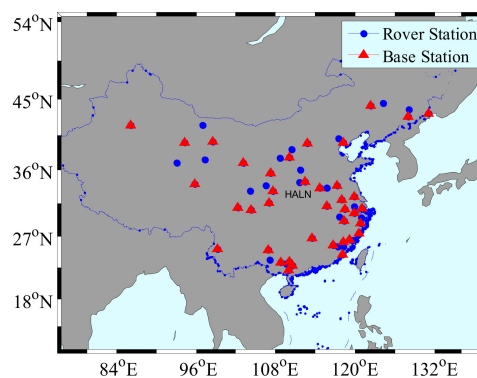


Figure 1. Distribution of the 60 stations used for observations collection in China.

To assess the benefits of ambiguity resolution when using GPS + BDS, we performed PPP ambiguity resolution for all 20 rover stations using data from a seven-day period. The daily observations were divided into 24 pieces composed of hourly sets; therefore, there were generally 168 hourly solutions for each station, which gave an overall total of 3360 solutions if there were no data losses. We assumed that the ambiguities could be fixed to the correct integers using the daily observations, and then the hourly ambiguities were compared with the daily “truth” to check its correctness. The WL ambiguity was fixed by rounding using a threshold of 0.25 cycles [5,6,41]. Because of the strong correlation, the least-squares ambiguity decorrelation adjustment (LAMBDA) method was used to search the NL ambiguity, and a ratio test was used to validate the ambiguity resolution using a threshold of 2.0 [14,18]. The initial fixing time attained in each hourly session was recorded and analyzed and we then obtained the fixing percentages for different observation durations via calculation of the cumulative distribution of the initial fixing times.

4. Results

In this section, we first present the results of real-time FCB estimation using the traditional method, and the effects of the orbit errors on both WL and NL FCB estimation are analyzed based on examination of the corresponding residuals. We then present the results of NL FCB estimation using the proposed method, and the estimated orbit errors and the residuals are also presented and analyzed. Finally, the improvements contributed by use of the proposed FCB estimation strategy to real-time PPP-IAR are analyzed.

4.1. Effects of Orbit Errors on FCB Estimation

Figure 2 shows the distributions of the a posteriori residuals of the WL FCB estimation with daily WL float ambiguities from all 40 reference stations during the seven-day period. If the ambiguities have an integer nature, the a posteriori residuals should obey a zero mean normal distribution. The distributions show that 96.6% of the WL residuals are within 0.15 cycles for GPS satellites, with a corresponding figure of 94.8% for the IGSO and MEO satellites, while more than 98% are within 0.25 cycles for both. This indicates the high consistency of the fractional parts of the WL float ambiguities for both the GPS satellites and the IGSO and MEO satellites of the BDS. However, because of the large multipath effects of the GEO satellites at low elevation angles [18,42], the residuals of the GEO satellites of the BDS are larger, but they still have 87.8% of the WL residuals within 0.25 cycles, which can satisfy the ambiguity resolution requirements.

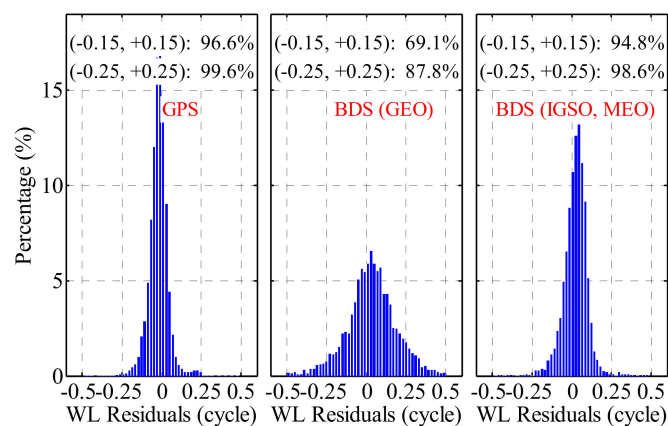


Figure 2. Distributions of the a posteriori residuals of the daily wide-lane (WL) ambiguities.

As an example, Figure 3 presents the time series of the NL residuals for two GEO, two IGSO, and two MEO satellites in the BDS system. For the two GEO satellites, the orbit errors are so large that

their residuals are evenly distributed within ± 0.5 cycles. From 1:00 to 8:00, the orbit error of C07 is very small, and the corresponding residuals are almost within ± 0.06 cycles. However, from 8:00 onwards, the orbit error increases, and the residuals then exceed 0.2 cycles for some of the stations. For C11, the residuals are also a little large and are distributed within ± 0.16 cycles. In contrast, for C08 and C12, the orbit errors are so large that the residuals are distributed within ± 0.45 cycles.

Figure 4 shows the distributions of the a posteriori residuals of the NL float ambiguities from all 40 reference stations during the seven-day period. The distributions show that 93.3% and 97.9% of the residuals are within ± 0.1 and ± 0.2 cycles for the GPS satellites, respectively. However, the residuals for the BDS GEO satellites are so large that only 60.6% of these residuals are within ± 0.2 cycles. The residuals for the BDS IGSO and MEO satellites are much smaller, but the percentages that lie within ± 0.1 and ± 0.2 cycles are still lower than those of the GPS satellites by 5.8% and 2.7%, respectively. These large residuals indicate that the precision of the estimated FCB is very poor and thus cannot be used for PPP ambiguity resolution.

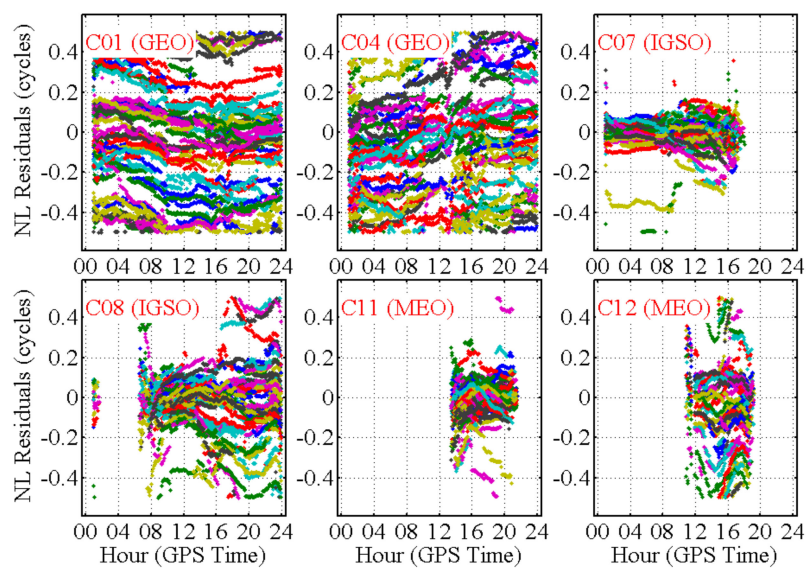


Figure 3. Time series of the a posteriori residuals of the NL ambiguities when using the traditional method on day of the year (DOY) 079 of 2015.

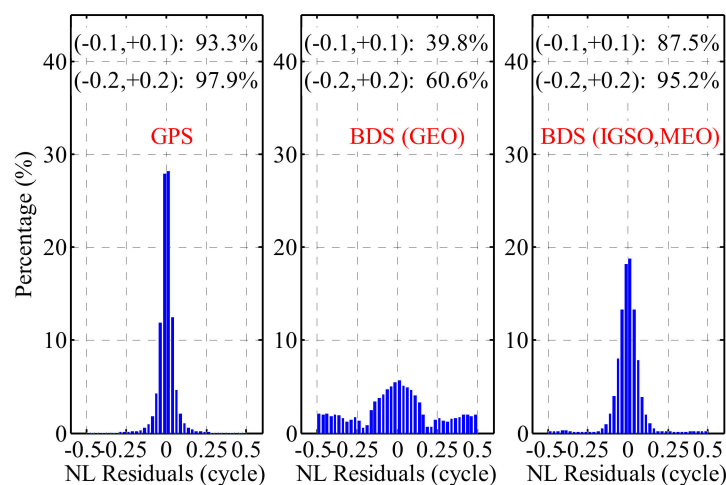


Figure 4. Distributions of the a posteriori residuals of the NL ambiguities when using the traditional method.

4.2. NL FCB Estimation When Considering Orbit Errors

In this subsection, the results of FCB estimation based on consideration of the orbit error are presented, and Figure 5 shows the estimated orbit errors of the six satellites corresponding to those shown in Figure 3. The figures show that the orbit errors in the Z direction of C01 and that in the Y direction of C04 exceed 1.5 and 2.0 m, respectively, which explains the large residuals shown in Figure 3. The orbit errors of C07 are very small over the period from 1:00 to 8:00 but they increase from 8:00 onwards, reaching up to 0.2 m in the X direction. The X direction orbit error for C11 also reaches 0.2 m. For C08 and C12, for which the NL residuals are both within ± 0.45 cycles, the orbit error can reach as much as 0.4 m. This is the reason why their NL residuals are much larger than those of C07 and C11. It should also be noted that the orbit error remains very stable over a short span and can be updated at intervals of 15 min or even longer.

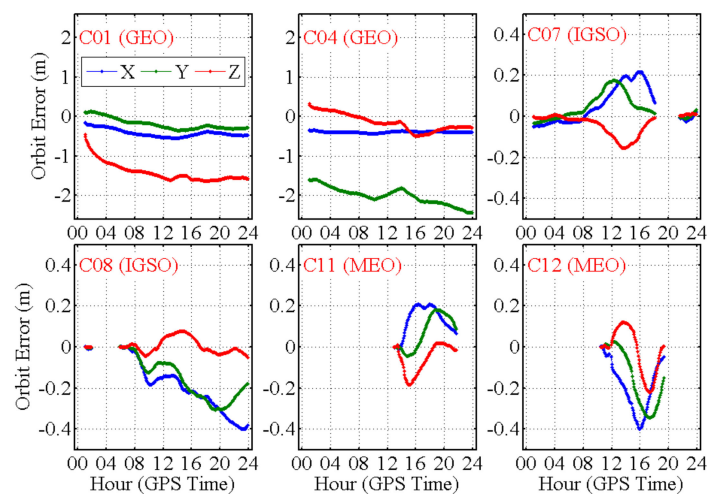


Figure 5. Time series of the estimated orbit errors on DOY 079 of 2015.

Figure 6 shows the corresponding NL residuals when considering the orbit errors. When compared with Figure 3, the impact of the orbit errors on NL FCB estimation is eliminated when the proposed method is used; more than 90% of the residuals are within ± 0.1 cycles for each satellite.

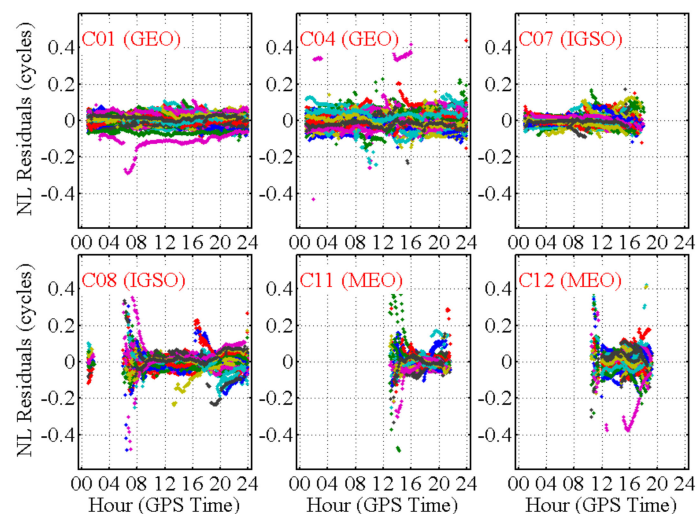


Figure 6. Time series of the a posteriori residuals of the NL ambiguities when using the new strategy on DOY 079 of 2015.

Figure 7 presents the distributions of the a posteriori residuals of the NL float ambiguities from all reference stations during the seven-day period. The figures show that more than 94% of the residuals fall within ± 0.1 cycles for the GPS satellites and for each type of the BDS satellites; under the criterion of ± 0.2 cycles, however, the corresponding percentage exceeded 97%. From the analysis above, the effect of orbit errors on BDS NL FCB estimation has been eliminated using the proposed method, and thus BDS PPP-IAR can be performed on large scales.

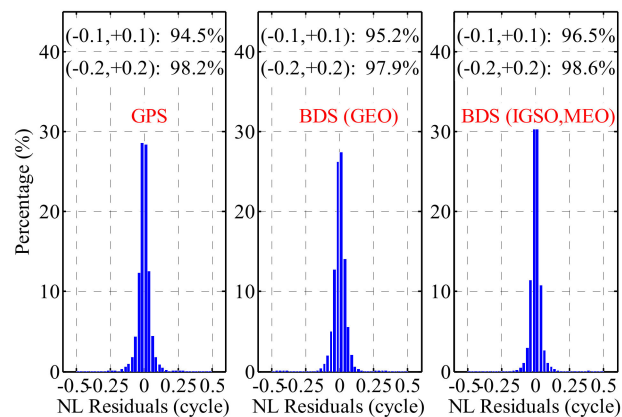


Figure 7. Distributions of the a posteriori residuals of the NL ambiguities when considering the orbit errors.

4.3. PPP-IAR Performance Analysis

We performed kinematic PPP-IAR for all hourly observations from the 20 rover stations using three models: GPS-only, GPS + BDS without consideration of the orbit error, and GPS + BDS with consideration of the orbit error. The fixing percentages at the different observation durations are shown in Figure 8, while typical values for observation durations of 5, 10, and 20 min are given in Table 4. When compared with the GPS-only solution, addition of BDS without consideration of the orbit corrections causes the fixing percentage to be severely degraded from 46.25 to 4.77% at the observation duration of 20 min. When the orbit corrections are considered, the fixing percentage improves significantly from 4.27 to 64.56% at an observation duration of 5 min, and from 46.25 to 91.73% at an observation duration of 20 min.

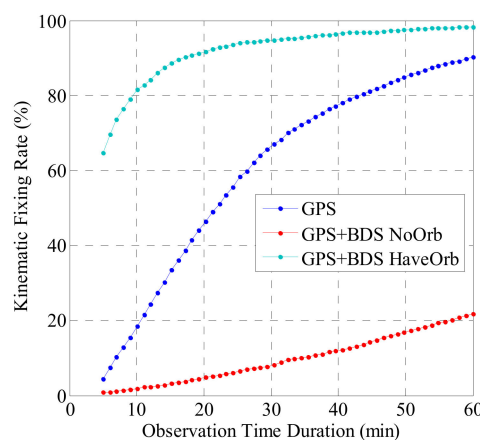
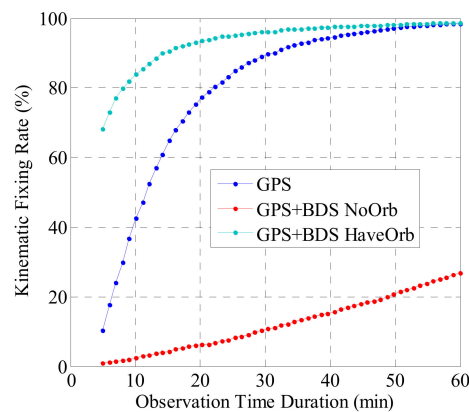


Figure 8. Fixing percentages for various observation durations for kinematic PPP when using different strategies.

Table 4. Fixing percentages for various observation durations for kinematic PPP when using different strategies.

Time (min)	GPS Only (%)	GPS + BDS	
		NoOrb (%)	HaveOrb (%)
05	4.27	0.78	64.56
10	18.33	1.78	81.53
20	46.25	4.77	91.73

The fixing percentages in static PPP-IAR at different observation durations are shown in Figure 9, while typical values for the observation durations of 5, 10 and 20 min are given in Table 5. When compared with the kinematic solution, the fixing percentage of the GPS-only solution improves significantly, i.e., from 46.25 to 77.29% for an observation duration of 20 min. However, for the GPS + BDS approach when considering the orbit corrections, the improvement from the static to the kinematic solution is less than 4% for the different observation durations. It should be noted that if we do not consider the orbit corrections, then the fixing percentage for GPS + BDS is also very small in the static solution.

**Figure 9.** Fixing percentages for various observation durations for static PPP when using different strategies.**Table 5.** Fixing percentages for various observation durations for static PPP when using different strategies.

Time (min)	GPS Only (%)	GPS + BDS	
		NoOrb (%)	HaveOrb (%)
05	10.33	0.91	68.17
10	42.44	2.49	84.01
20	77.29	6.05	93.48

For further assessment of the performance of the proposed method, we calculated the fixing percentages for an observation duration of 20 min for each station, where the results are shown in Figure 10 for the kinematic solution and in Figure 11 for the static solution. The stations are arranged in terms of the distance from each station to the central station (HALN). The fixing percentages for GPS-only are between 33% and 60% for each station in kinematic PPP and improved to percentages of between 67% and 90%. If we add BDS without the orbit corrections, the percentages are severely degraded to less than 12% for all stations. After use of the orbit corrections, the fixing percentages of GPS + BDS exceed 79% for all stations and average 92.2% in the kinematic solution, while they exceed 84% for all stations and average 94.1% in the static solution.

Table 6 lists the position RMS for each fixed epoch for GPS and GPS + BDS kinematic PPP. For GPS + BDS, because the ambiguity fixing percentage is very low without use of the orbit corrections, we only calculated the RMS with the orbit corrections. On average, the position RMS is 0.85, 0.69 and 2.94 cm for GPS in the north, east and up directions, respectively. When BDS was added, these RMS values were reduced to 0.77, 0.67 and 2.88 cm, with improvements of 9.4%, 2.9%, and 2.0%, respectively.

Table 6. Position RMS (cm) for kinematic ambiguity fixed PPP solutions.

	North	East	Up
GPS	0.85	0.69	2.94
GPS + BDS HaveOrb	0.77	0.67	2.88

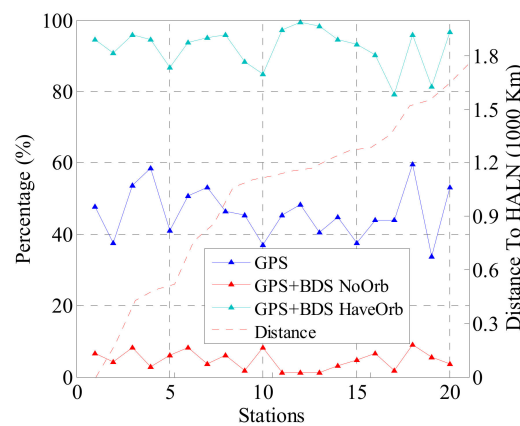


Figure 10. Fixing percentages for kinematic PPP when using different strategies for an observation duration of 20 min on each day.

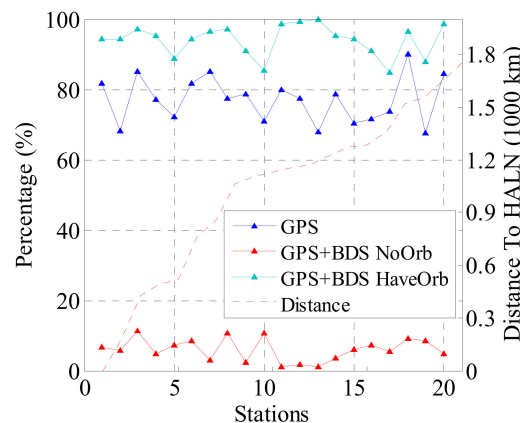


Figure 11. Fixing percentages for static PPP when using different strategies for an observation duration of 20 min on each day.

5. Discussions

To provide further confirmation of the origins of the large residuals shown in Figure 3, we selected the epoch in which the residuals were at their largest for each satellite and visualized the relationships between the NL residuals and the distance to the central station (HALN) as shown in Figure 12. For C01 and C04, the epoch was 9:00:00; for C07, the epoch was 13:00:00; and for C08, the epoch was 20:00:00, while it was 16:00:00 for both C11 and C12. The figures show that for the GEO satellites, the NL residuals range between -0.5 and $+0.5$ and show no relationship to the distance to the central

station. For the IGSO and MEO satellites, however, for which the NL residuals are not as large as those of the GEO satellites, the residuals gradually increase with increasing distance to the central station.

For comparison to Figure 12, Figure 13 gives the results when the orbit errors were considered. After consideration of the orbit errors, the residuals are all within 0.1 cycles for each satellite and for all stations, with the exception of three outliers. No trend between the size of the residual and the distance to the central station of the network is shown. Because the station-specific errors (i.e., troposphere errors and multipath errors) will not present such significant location-specific regulation (see Figure 12) and because these errors will not disappear when the orbit errors are considered (see Figure 13), it can thus be confirmed that the large residuals shown in Figure 3 are caused by large orbit errors and the proposed method can thus work appropriately in eliminating the effects of large orbit errors on NL FCB estimation.

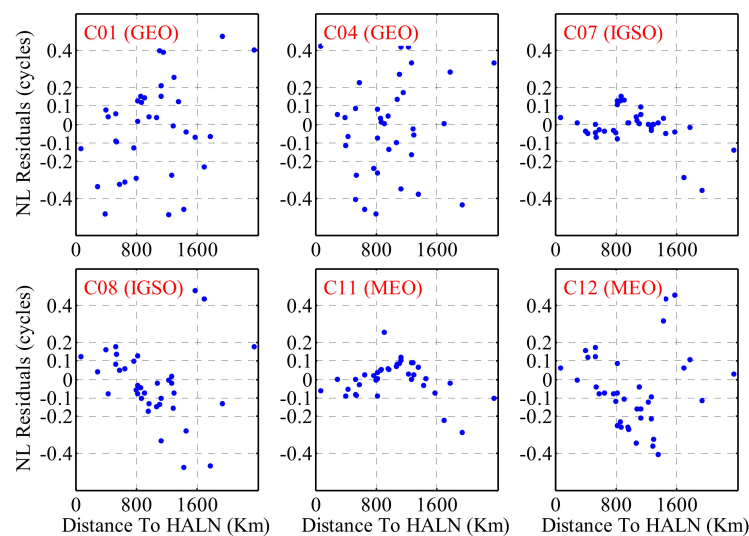


Figure 12. A posteriori residuals of the NL ambiguities when using the traditional method with respect to distance to the central station of the network (HALN).

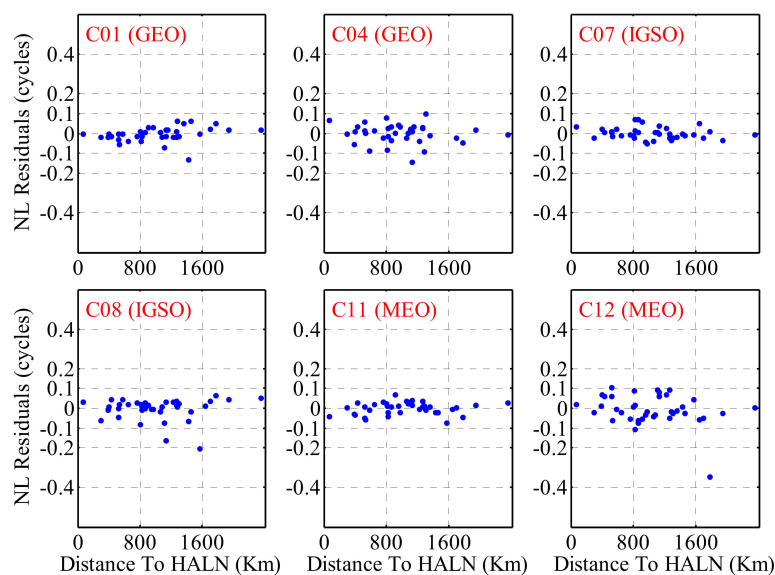


Figure 13. A posteriori residuals of the NL ambiguities when using the proposed strategy with respect to the distance to the central station of the network (HALN).

6. Conclusions and Outlook

With its five GEO, five IGSO and four MEO satellites, the BDS system plays an important role in PPP in the Asia-Pacific region. However, because of the lack of sufficiently well-distributed tracking stations and a poorly developed solar radiation pressure model, the orbit precision of the BDS satellites is low when compared with that of the GPS satellites [24,25,27]; this is particularly true for the GEO satellites, which remain nearly stationary relative to the ground tracking stations. This poor orbit precision will affect the NL FCB estimation results of BDS satellites quite severely. This paper proposes a strategy for estimation of the GPS + BDS FCB based on consideration of the orbit error, and has demonstrated a GPS + BDS FCB estimation approach along with PPP ambiguity resolution in a simulated real-time model using the stations distributed across China.

In general, more than 98% of the a posteriori residuals of the WL ambiguities are within ± 0.25 cycles for the GPS, IGSO, and MEO satellites; while this figure falls to 87% for the GEO satellites. After the orbit errors were taken into consideration, more than 94% of the NL a posteriori residuals were within ± 0.1 cycles for all satellite types. The contribution of the BDS observations to GPS-only PPP-IAR has also been investigated. In kinematic PPP, within a 5-min period, the fixing percentage for the solo GPS solution was only 4.27%; however, when the BDS was added, the percentage improved significantly to 64.56%. For observation periods of 10 min and 20 min, the fixing percentages were 18.33% and 46.25%, respectively, for the solo GPS, but rose to 81.53% and 91.73%, respectively, when using the GPS + BDS solution. With obvious contrast, if the GPS + BDS mode is used without consideration of the orbit errors, the fixing percentage only reaches 1.78% for a time period of 6 min and reaches 4.77% for both 10-min and 20-min observation periods. After the ambiguities are correctly fixed, the RMS position accuracy is degraded to 0.77, 0.67, and 2.88 cm for the north, east, and up directions, respectively, with improvements of 9.4%, 2.9%, and 2.0% when compared with the GPS-only solution.

Based on the scale factor, a wider tracking network distribution enables better orbit error estimation. The network used in this study covers an area with a radius of 1500 km, which is relatively small when compared with the globally distributed network of tracking stations. Therefore, with this network, we can only solve “part” of the orbit error, which may only satisfy the requirements for PPP-IAR within this network. Using greater numbers of Multi-GNSS Experiment (MGEX) stations [43], we intend to investigate the performance of the proposed method over larger networks. In addition, the higher-order ionospheric delays and the bending effect both affect the PPP solutions [44]. In this study, we have not considered the higher-order ionospheric delays as part of our PPP processing. Therefore, in future work, we will also consider these higher-order ionospheric delays and analyze their contributions to PPP-IAR performance.

Author Contributions: Y.L. conceptualized the initial idea and experimental design. J.Z. performed the experiments. S.Y. wrote the main manuscript text. W.S. helped with data collection and analysis of the results.

Acknowledgments: This work was partially supported by the National Natural Science Foundation of China (No. 41704033), the Shenzhen Future Industry Development Funding Program (No. 201607281039561400), the Shenzhen Scientific Research and Development Funding Program (No. JCYJ20170818092931604), and the Research Program of Shenzhen S&T Innovation Committee (No. JCYJ20170412105839839).

Conflicts of Interest: The authors declare no conflict of interest.

References

1. Zumberge, J.; Heflin, M.; Jefferson, D.; Watkins, M.; Webb, F. Precise point positioning for the efficient and robust analysis of GPS data from large networks. *J. Geophys. Res.* **1997**, *102*, 5005–5017. [[CrossRef](#)]
2. Kouba, J.; Héroux, P. Precise point positioning using IGS orbit and clock products. *GPS Solut.* **2001**, *5*, 12–28. [[CrossRef](#)]
3. Bisnath, S.; Gao, Y. Current state of precise point positioning and future prospects and limitations. In *Observing our Changing Earth*; IAG Symposium Series; Springer: Berlin/Heidelberg, Germany, 2007; Volume 133, pp. 615–624.

4. Dow, J.; Neilan, R.; Rizos, C. The international GNSS service in a changing landscape of global navigation satellite systems. *J. Geod.* **2009**, *83*, 191–198. [[CrossRef](#)]
5. Ge, M.; Gendt, G.; Rothacher, M.; Shi, C.; Liu, J. Resolution of GPS carrier phase ambiguities in precise point positioning (PPP) with daily observations. *J. Geod.* **2008**, *82*, 389–399. [[CrossRef](#)]
6. Geng, J. Rapid Integer Ambiguity Resolution in GPS Precise Point Positioning. Ph.D. Thesis, University of Nottingham, Nottingham, UK, 2010; p. 153.
7. Collins, P.; Lahaye, F.; Héroux, P.; Bisnath, S. Precise point positioning with AR using the decoupled clock model. In Proceedings of the ION GNSS-2008, Savannah, GA, USA, 16–19 September 2008; pp. 1315–1322.
8. Laurichesse, D.; Mercier, F.; Berthias, J.P.; Broca, P.; Cerri, L. Integer ambiguity resolution on undifferenced GPS phase measurements and its application to PPP and satellite precise orbit determination. *Navigation* **2009**, *56*, 135–149. [[CrossRef](#)]
9. Gabor, M.J.; Nerem, R.S. GPS carrier phase AR using satellite-satellite single difference. In Proceedings of the ION GNSS-1999, Nashville, TN, USA, 14–17 September 1999; pp. 1569–1578.
10. Geng, J.; Teferle, F.N.; Meng, X.; Dodson, A.H. Towards PPP-RTK: Ambiguity resolution in real-time precise point positioning. *Adv. Space Res.* **2011**, *47*, 1664–1673. [[CrossRef](#)]
11. Jokinen, A.; Feng, S.; Schuster, W.; Ochieng, W.; Hide, C.; Moore, T.; Hill, C. GLONASS aided GPS ambiguity fixed precise point positioning. *J. Navig.* **2013**, *66*, 399–416. [[CrossRef](#)]
12. Li, P.; Zhang, X. Integrating GPS and GLONASS to accelerate convergence and initialization times of precise point positioning. *GPS Solut.* **2014**, *18*, 461–471. [[CrossRef](#)]
13. Geng, J.; Shi, C. Rapid initialization of real-time PPP by resolving undifferenced GPS and GLONASS ambiguities simultaneously. *J. Geod.* **2017**, *91*, 1–14. [[CrossRef](#)]
14. Liu, Y.; Ye, S.; Song, W.; Lou, Y.; Gu, S.; Li, Q. Rapid PPP Ambiguity Resolution Using GPS+GLONASS Observations. *J. Geod.* **2016**. [[CrossRef](#)]
15. Tegedor, J.; Liu, X.; Jong, K.; Goode, M.; Øvstedal, O.; Vigen, E. Estimation of Galileo Uncalibrated Hardware Delays for Ambiguity-Fixed Precise Point Positioning. *Navigation* **2016**, *63*, 173–179. [[CrossRef](#)]
16. Cai, C.; Gao, Y.; Pan, L.; Zhu, J. Precise point positioning with quad-constellations: GPS, BeiDou, GLONASS and Galileo. *Adv. Space Res.* **2015**, *56*, 133–143. [[CrossRef](#)]
17. Li, X.; Ge, M.; Dai, X.; Ren, X.; Fritsche, M.; Wickert, J.; Schuh, H. Accuracy and reliability of multi-GNSS real-time precise positioning: GPS, GLONASS, BeiDou, and Galileo. *J. Geod.* **2015**, *89*, 607–635. [[CrossRef](#)]
18. Liu, Y.; Ye, S.; Song, W.; Lou, Y.; Chen, D. Integrating GPS and BDS to shorten the initialization time for ambiguity-fixed PPP. *GPS Solut.* **2016**. [[CrossRef](#)]
19. Shi, C.; Zhao, Q.; Li, M.; Tang, W.; Hu, Z.; Lou, Y.; Zhang, H.; Niu, X.; Liu, J. Precise orbit determination of BeiDou Satellites with precise positioning. *Sci. China Earth Sci.* **2012**, *55*, 1079–1086. [[CrossRef](#)]
20. Ge, M.; Zhang, H.; Jia, X.; Song, S.; Wickert, L. What is achievable with the current COMPASS Constellations? In Proceedings of the ION GNSS 2012, Institute of Navigation, Nashville, TN, USA, 17–21 September 2012; pp. 331–339.
21. Steigenberger, P.; Hugentobler, U.; Hauschild, A.; Montenbruck, O. Orbit and clock analysis of compass GEO and IGSO satellites. *J. Geod.* **2013**, *87*, 515–525. [[CrossRef](#)]
22. Zhao, Q.; Guo, J.; Li, M.; Qu, L.; Hu, Z.; Shi, C.; Liu, J. Initial results of precise orbit and clock determination for COMPASS navigation satellite system. *J. Geod.* **2013**, *87*, 475–486. [[CrossRef](#)]
23. He, L.; Ge, M.; Wang, J.; Wickert, J.; Schuh, H. Experimental study on the precise orbit determination of the BeiDou navigation satellite system. *Sensors* **2013**, *13*, 2911–2928. [[CrossRef](#)] [[PubMed](#)]
24. Lou, Y.; Liu, Y.; Shi, C.; Wang, B.; Yao, X.; Zheng, F. Precise orbit determination of BeiDou constellation: Method comparison. *GPS Solut.* **2016**, *20*, 259–268. [[CrossRef](#)]
25. Kazmierski, K.; Sośnica, K.; Hadas, T. Quality assessment of multi-gnss orbits and clocks for real-time precise point positioning. *GPS Solut.* **2018**, *22*, 11. [[CrossRef](#)]
26. Dach, R.; Schaer, S.; Lutz, S.; Bock, H.; Orliac, E.; Prange, L.; Thaller, D.; Mervart, L.; Jäggi, A.; Beutler, G.; et al. *CODE Analysis Center Technical Report 2014*; International GNSS Service: Technical Report 2014; Dach, R., Jean, Y., Eds.; IGS Central Bureau: Pasadena, CA, USA, 2015; p. 2134.
27. Li, X.; Chen, X.; Ge, M.; Schuh, H. Improving multi-GNSS ultra-rapid orbit determination for real-time precise point positioning. *J. Geod.* **2018**. [[CrossRef](#)]
28. Montenbruck, O.; Steigenberger, P.; Hauschild, A. Broadcast versus precise ephemerides: A multi-gnss perspective. *GPS Solut.* **2015**, *19*, 321–333. [[CrossRef](#)]

29. Wanninger, L.; Beer, S. BeiDou satellite-induced code pseudorange variations: Diagnosis and therapy. *GPS Solut.* **2015**, *19*, 639–648. [[CrossRef](#)]
30. Lou, Y.; Gong, X.; Gu, S.; Zheng, F.; Feng, Y. Assessment of code bias variations of bds triple-frequency signals and their impacts on ambiguity resolution for long baselines. *GPS Solut.* **2017**, *21*, 177–186. [[CrossRef](#)]
31. Wu, J.; Wu, S.; Hajj, G.; Bertiger, W.; Lichten, S. Effects of antenna orientation on GPS carrier phase. *Manuscr. Geod.* **1993**, *18*, 91–98.
32. Geng, J.; Meng, X.; Dodson, A.; Teferle, F. Integer ambiguity resolution in precise point positioning: Method comparison. *J. Geod.* **2010**, *84*, 569–581. [[CrossRef](#)]
33. Shi, J.; Gao, Y. A comparison of three PPP integer ambiguity resolution methods. *GPS Solut.* **2014**, *18*, 519–528. [[CrossRef](#)]
34. Hatch, R. The synergism of GPS code and carrier measurements. In Proceedings of the Third International Symposium on Satellite Doppler Positioning at Physical Sciences Laboratory of New Mexico State University, Las Cruces, NM, USA, 8–12 February 1982; Volume 2, pp. 1213–1231.
35. Melbourne, W.G. The case for ranging in GPS-based geodetic systems. In Proceedings of the First International Symposium on Precise Positioning with the Global Positioning System, Rockville, MD, USA, 15–19 April 1985.
36. Wübbena, G. Software developments for geodetic positioning with GPS using TI-4100 code and carrier measurements. In Proceedings of the First International Symposium on Precise Positioning with the Global Positioning System, Rockville, MD, USA, 15–19 April 1985.
37. Liu, Y.; Ye, S.; Song, W.; Li, Q. Estimating the orbit error of BeiDou GEO satellites to improve the performance of multi-GNSS PPP ambiguity resolution. *GPS Solut.* **2018**, doi:10.1007/s10291-018-0751-9.
38. Petit, G.; Luzum, B.; Al, E. *IERS Conventions*; IERS Technical Note; IERS Central Bureau: Frankfurt am Main, Germany; 2010; Volume 36, pp. 1–95.
39. Boehm, J.; Niell, A.; Tregoning, P.; Schuh, H. Global mapping function (GMF): A new empirical mapping function based on numerical weather model data. *Geophys. Res. Lett.* **2006**, *33*, L07304. [[CrossRef](#)]
40. Wang, G.; de Jong, K.; Zhao, Q.; Hu, Z.; Guo, J. Multipath analysis of code measurements for BeiDou geostationary satellites. *GPS Solut.* **2015**, *19*, 129–139. [[CrossRef](#)]
41. Liu, J.; Ge, M. PANDA software and its preliminary result of positioning and orbit determination. *Wuhan Univ. J. Nat. Sci.* **2003**, *8*, 603–609.
42. Yi, W.; Song, W.; Lou, Y.; Shi, C.; Yao, Y.; Guo, H.; Chen, M.; Wu, J. Improved method to estimate undifferenced satellite fractional cycle biases using network observations to support PPP ambiguity resolution. *GPS Solut.* **2017**, *21*, 1369–1378. [[CrossRef](#)]
43. Montenbruck, O.; Steigenberger, P.; Prange, L.; Deng, Z.; Zhao, Q.; Perosanz, F. The multi-GNSS experiment (MGEX) of the international GNSS service (IGS)—Achievements, prospects and challenges. *Adv. Space Res.* **2017**, *59*, 1671–1697. [[CrossRef](#)]
44. Hadas, T.; Krypiak-Gregorczyk, A.; Hernández-Pajares, M.; Kaplon, J.; Paziewski, J.; Wielgosz, P.; Garcia-Rigo, A.; Kazmierski, K.; Sosnica, K.; Kwasniak, D.; et al. Impact and implementation of higher-order ionospheric effects on precise gnss applications. *J. Geophys. Res. Solid Earth* **2017**, *122*, 9420–9436. [[CrossRef](#)]

